ACS APPLIED ELECTRONIC MATERIALS

pubs.acs.org/acsaelm Article

THz Generation from the Topological Nodal Line Semimetal Co_2MnGa

Luca Tomarchio, Sen Mou, Lorenzo Mosesso, Anastasios Markou, Edouard Lesne, Claudia Felser, and Stefano Lupi*

Cite This: *ACS Appl. Electron. Mater.* 2023, 5, 1437−1443 Read Online

ACCESS | Metrics & More | Article Recommendations | Supporting Information

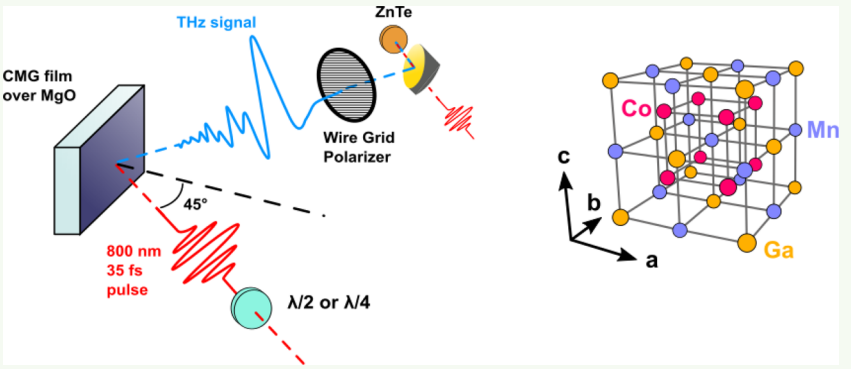

ABSTRACT: Nonlinear optical spectroscopy is a fundamental probe for the investigation of topological effects in quantum materials. In this paper, we report on the terahertz (THz) emission from thin films at various thicknesses of the magnetic topological nodal semimetal Co_2MnGa (CMG) when excited by femtosecond optical pulses. Experimental results suggest the presence of multiple THz generation mechanisms, originating from both bulk and surface states of CMG. The former is explained in terms of a photon-drag effect as induced by radiation pressure. The latter emission mechanism instead appears to be related to the photovoltaic effect coming from the topological surface states. This interplay between generation mechanisms indicates that Co_2MnGa topological nodal semimetals are a valuable platform for THz emitter devices.

KEYWORDS: *THz emission, spectroscopy, topology, magnetism, photogalvanic effect*

INTRODUCTION

Since the breakthrough discovery of topological materials, several intriguing effects related to the topological nature of their electronic band structure have been highlighted theoretically and experimentally. Magnetoelectric and thermoelectric effects, like the anomalous Hall and Nernst effects,[1−4] or enhanced nonlinear optical responses, like multiple harmonic generation (MHG)[5−7] and linear/circular photogalvanic effects (L/CPGE),[8,9] are just a few of the novel properties found in these materials that can be exploited in future electro-optical applications. More recently, topological materials breaking time-reversal symmetry provide novel topological phases of matter, like the magnetic topological insulators[10−12] and semimetals[13−15] and the axion insulators.[1]

The full-Heusler alloy Co_2MnGa (CMG) is a metallic ferromagnet with a Curie temperature >600 K that crystallizes in the cubic Cu_2MnAl-type structure with space group $Fm\bar{3}m$[16,17] (see Figure 1a). CMG has been theoretically predicted[18,19] and experimentally proved[20] to be a magnetic topological nodal line semimetal, showing a complex structure where the valence and conduction bands cross along arbitrarily intertwined nodes.[21,22] Moreover, the intricate nodal structure of CMG was revealed to contain Hopf links and show unconventional density of states and band structure,[18,20] which have led to enhanced perspectives for nonlinear optical responses and higher harmonic generation (HHG).[23−25]

Despite the promising properties of CMG, not much is known about its electronic properties.[26−30] Moreover, it is so far unclear what distinct experimental signature corresponds to the nontrivial band topology.[31] Anomalous Hall[32] and Nernst[33,34] effects have been reported as a measure of the topological features, along with THz Faraday rotation[35] and spin-current generation.[36] Recent theoretical results have suggested that the HHG effect, related to the exotic nodal geometry, might be enhanced drastically by the Berry

Received: October 10, 2022
Accepted: February 9, 2023
Published: March 8, 2023

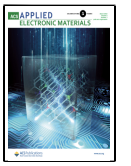

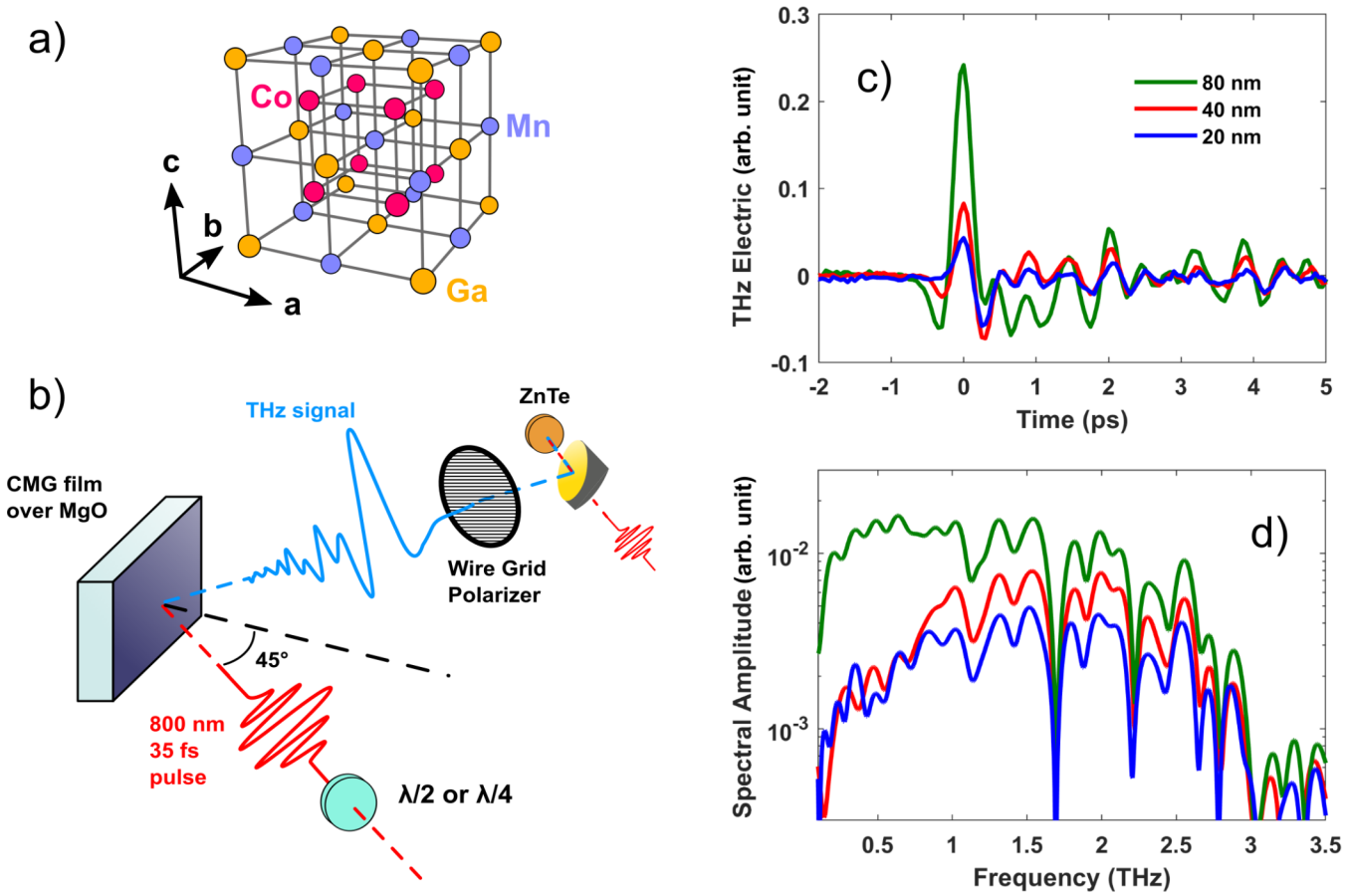

Figure 1. THz emission by optical excitation in Co_2MnGa thin films. (a) Co_2MnGa cubic unit cell. The structure is a result of four interpenetrating face-centered-cubic (FCC) lattices (Heusler alloy structure). The arrows indicate the crystal axes. (b) Experimental setup for the generation and detection of THz waves from CMG thin films. Films are illuminated in a 45° reflection geometry by a 800 nm ultrashort pulse with tunable fluence and polarization. The THz detection is achieved through an electro-optical coupling by a ZnTe nonlinear crystal. (c) THz electric field in time as emitted by three CMG films of different thicknesses. (d) Spectral amplitudes of the THz signals, revealing the frequency emission band. Sharp dips are associated with water vapor absorptions during propagation in air.

curvature.[31] A distinct mechanism coupling to the topology of the band structure is the production of photocurrents (shift currents) through the linear/circular photogalvanic mechanism.[6,8,9] In Weyl semimetals[37−40] and topological insulators,[41,42] it has been demonstrated how this effect generates polarization-sensitive THz radiation from both the bulk and surface states. In centrosymmetric materials like CMG, where parity conservation forbids bulk second-order nonlinear phenomena, THz emission is an optimal probe of the surface states, thus giving a direct probe of the topological features of the material.

In this work, we study the THz emission by high-quality CMG thin films with different thicknesses (20, 40, and 80 nm), grown on MgO(100) substrates, after being pumped by a 800 nm femtosecond optical pulse. The pump polarization was tuned from linear to circular, highlighting different mechanisms behind the whole THz generation. In particular, we distinguish a sub-THz generation coming from the topological surface states and explained in terms of the photogalvanic effect, as well as an emission at higher frequencies scaling linearly with the thickness and hence attributed to the bulk. Although very little is know about the bulk THz emission in parity-conserved semimetals, its origin can be found in the photon-drag effect, as already observed for metallic thin films and graphene.[43,44] The interplay between different generation mechanisms promotes Co_2MnGa topological nodal semimetal as a valuable platform for the production of tunable THz radiation.

EXPERIMENTAL SECTION

Thin Films Growth. Thin films of Co_2MnGa with thicknesses of 20, 40, and 80 nm were grown epitaxially, on (001)-oriented MgO single-crystal substrates, using a BESTEC ultrahigh vacuum magnetron sputtering system. Prior to the deposition, the chamber was evacuated to a base pressure of $<8 \times 10^{-9}$ mbar, while the process gas (Ar 5 N) pressure was set to 3×10^{-3} mbar. For the growth of the films, we used an equiatomic compound $Mn_{50}Ga_{50}$ (5.08 cm) and high-purity elemental metal Co and Mn (5.08 cm) sources in a confocal geometry, applying 20, 34, and 6 W dc power, respectively. The target-to-substrate distance was fixed at 18 cm, and the substrate was rotated with a speed of 20 rpm during deposition to ensure a homogeneous growth. The films were grown at 600 °C, followed by in situ postannealing at the same temperature for 30 min to improve the crystallinity of the films. To avoid oxidation of the films, an amorphous Si layer of 3 nm was deposited in situ at room temperature using a Si (5.08 cm) source and applying 60 W RF power.

THz Emission Spectroscopy Setup. THz emission spectroscopy on a CMG thin film has been performed by pumping the samples with a 800 nm ultrashort pulse (35 fs), as obtained by a Ti:sapphire amplifier (Coherent Verdi G-series), with a repetition rate of 1 kHz. The pulse is sent on the films at a 45° angle geometry, and the THz signal is collected in reflection by a series of parabolic mirrors. The

https://doi.org/10.1021/acsaelm.2c01376
ACS Appl. Electron. Mater. 2023, 5, 1437−1443

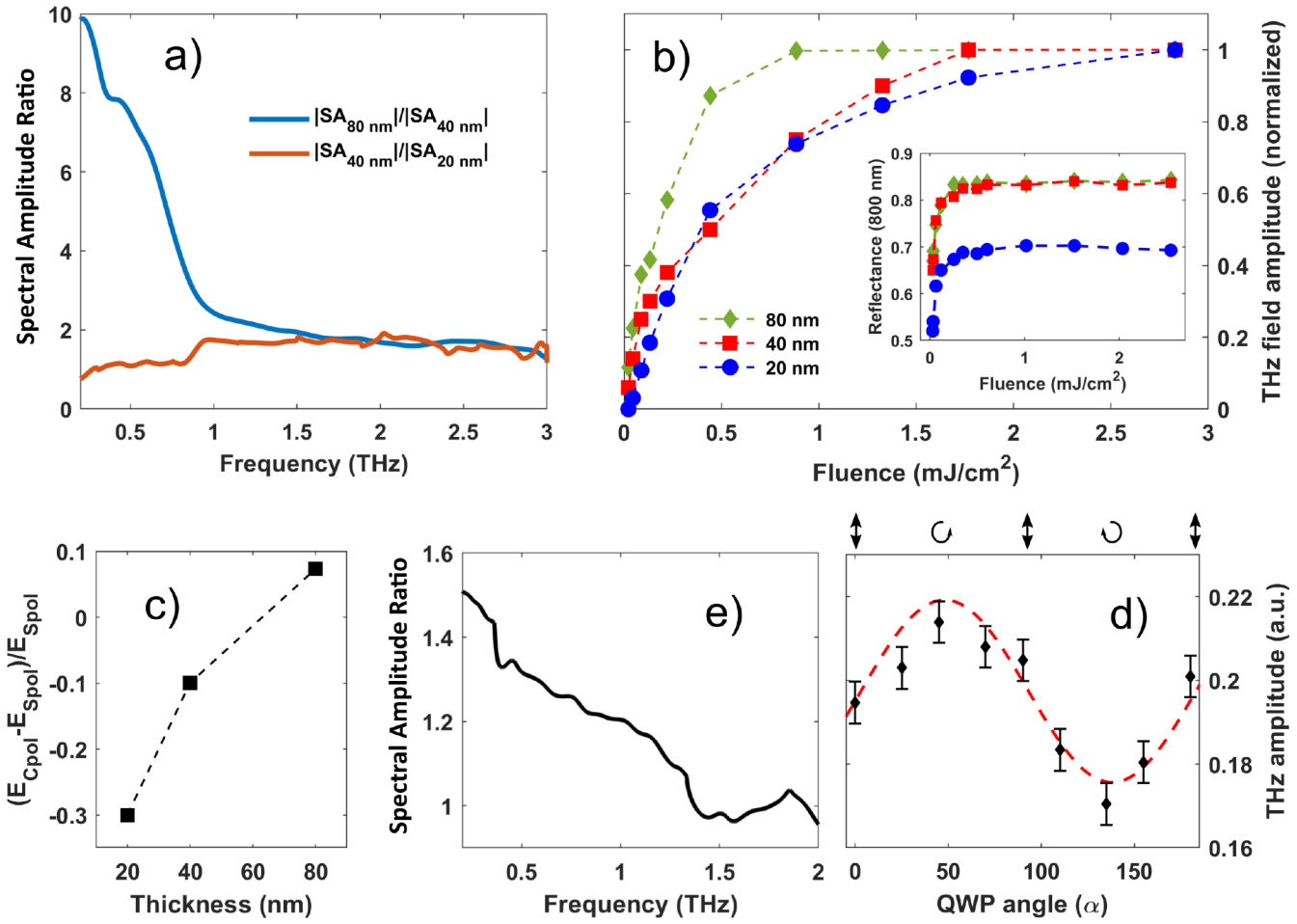

Figure 2. Fluence and polarization dependence of the THz emission from Co_2MnGa thin films. (a) Ratios between the 80 and 40 nm spectral amplitudes (blue) and between the 40 and 20 nm spectral amplitudes (red). (b) Fluence dependence of the emitted THz amplitude (peak-to-peak value). The inset shows the nonlinear enhancement of the reflectance of the film at a pumping wavelength of 800 nm. (c) Ratio between the THz peak-to-peak amplitude emitted after pumping with a linearly (*S*-polarized) and circularly polarized 800 nm pulse. (d) Ratio between the THz spectral amplitude generated by a 80 nm CMG film when pumped by a circularly over linearly (*S*-pol) polarized beam. (e) THz field amplitude from the 80 nm film after being illuminated by an optical pump with variable polarization, as modified by a quarter waveplate (of angle α). An angle $\alpha = 45°$ identifies a left-circularly polarized light, while $\alpha = 135°$ is a right-circularly polarized one. The sinusoidal red curve identifies a 2α fit.

signal is then sent to a 250 μm ZnTe crystal for the electro-optical detection by a balanced photodetector. The crystal orientation has been kept fixed for all measurements. The THz signal from the films has been compared to the THz generated in a transmission geometry by a second thicker (500 μm) ZnTe crystal. Half and quarter waveplates for the 800 nm signal have been used to tune the incident polarization, while a wire-grid polarizer has been used to filter the THz signal polarization.

RESULTS

High-quality epitaxial thin films of Co_2MnGa were grown in a BESTEC UHV magnetron sputtering system on MgO(001) single-crystal substrates and capped in situ with 3 nm Al, whose surface naturally oxidizes at ambient conditions. The details of the growth are provided in the Experimental Section. The cubic crystal structure of CMG is shown in Figure 1a. In this work, three films of 20, 40, and 80 nm thickness have been measured.

THz emission from CMG thin films was measured through the optical setup shown in Figure 1b and described in the Experimental Section. A femtosecond pulse, centered at 800 nm and provided by a Coherent Legend amplifier (7 mJ of pulse energy, 35 fs of pulse duration, and 1 kHz of repetition rate), was used to illuminate the thin films in a reflection geometry at a 45° angle of incidence. THz emitted radiation is focused on a ZnTe nonlinear crystal and detected by an electro-optical process.[45]

Figure 1c shows the THz field emitted by the three films with different thicknesses, illuminated by a linearly *S*-polarized optical pulse with a fluence of 1.77 mJ/cm^2. The terahertz intensity (from the 80 nm film) is ~3% of that measured using a 500 μm thick ZnTe crystal under identical conditions (same exciting laser, illuminated area, and fluence). Per unit thickness, the generation efficiency of the CMG film is hundreds of times higher than that of the ZnTe nonlinear crystal. Figure 1d shows the spectral amplitude (SA) of the THz signals obtained through a fast Fourier transform (FFT) algorithm. The sharp dips between 1 and 3 THz are associated with water absorption from the atmospheric air. Due to the limitation of the ZnTe detection band, the THz signal emitted from the 80 nm film was also measured through a GaP crystal that was able to detect the higher THz frequencies although it was less sensitive to the field intensity due to the lower electro-optic coefficient.[45] Even in this case, the emitted spectrum

https://doi.org/10.1021/acsaelm.2c01376
ACS Appl. Electron. Mater. 2023, 5, 1437−1443

shows a cutoff at nearly 3 THz, suggesting that the whole CMG THz emitted spectrum is confined below this frequency.

DISCUSSION

The THz emission described earlier provides fundamental information about topological effects in Co_2MnGa. Indeed, for nonlinear second-order responses (like the optical-rectification process), a noncentrosymmetric unit cell is required. This is not the case for CMG, which, having a cubic structure at room temperature (RT), keeps the parity symmetry intact while breaking the time-reversal one due to a Curie temperature >600 K. Therefore, one expects a major contribution in the THz emission from topological surface states, where the parity symmetry is broken. Instead, we observe a complex thickness dependence of the THz emission, revealing a further THz production mechanism originating from the bulk.

In Figure 2a we show the ratio between the THz spectral amplitudes of the three films (SA(80 nm)/SA(40 nm) blue curve, SA(40 nm)/SA(20 nm) red curve). The dependency of the THz field with thickness appears nontrivial across the full THz spectrum. SA(40 nm)/SA(20 nm) is nearly flat with a value ∼2 (doubled field) above 1 THz, in agreement with the thickness ratio. A similar result is found for the ratio between 80 and 40 nm. However, below this frequency, the emitted THz field increases rapidly for the 80 nm film. Thinner films of 20 and 40 nm do not host a valuable difference in their generation in this sub-THz range, while the 80 nm film shows a sharp increase (nearly a factor 10) in the THz generation emission.

From these measurements, we distinguish two mechanisms for THz generation in Co_2MnGa: a first mechanism, scaling linearly with thickness and therefore related to bulk carriers, which we associate to a (nontopological) photon-drag effect, and a surface mechanism mainly contributing to the sub-THz spectral region, whose properties suggest a topological origin as described below.

Further differences between the 80 nm and the thinner films can be observed in Figure 2b. Here, one shows the behavior of the THz electric field amplitude versus the pump fluence F. All films show a first linear increase with F further followed by a saturation behavior. However, the saturation effect is faster for the 80 nm film than the other two thicknesses, which behave very similarly. This difference cannot be linked to the bulk response, as suggested by the equal saturation fluence effect for the 80 and 40 nm film reflectance at 800 nm (see inset of Figure 2b), which is mainly determined by the bulk carriers. Indeed, the optical penetration depth at 800 nm is ∼50 nm, comparable to the film thickness. The faster THz saturation effect vs F in the 80 nm film can then be related to its surface contribution, being dominant with respect to the bulk response. The fluence dependence behavior of the 80 nm film, having a $\sqrt{F}$ functional form, can be compared to the results of a Floquet two-band model for the production of shift currents.[6] The plateau of the THz amplitude above 1 mJ/cm^2 can instead be linked to the filling of surface states because the flux of photons incident at this fluence (4×10^{15} cm^{-2}) is comparable to the surface density of carriers (∼10^{16} cm^{-2}).[27]

Polarization Analysis and Bulk THz Emission. As discussed previously, the emission above 1 THz, due to its scaling with thickness, can be associated with the CMG bulk. In this case, due to the cubic lattice structure of CMG and therefore to the corresponding parity conservation, the main THz emission mechanism can be attributed to the photon-drag effect.[46−49] This picture is supported by the polarization-sensitive measurements agreeing with a THz polarization mainly P-oriented ($\theta = 90°$), in accordance with a photon-drag generation mechanism where the photocurrents are generated by the transfer of momentum from the photons to the free electrons. The THz signal was probed after being transmitted by a rotating (θ) wire-grid polarizer from 0 to 180°, thus scanning the polarization properties of the THz beam. The Malus curves for the emitted THz light, as obtained by a linearly polarized optical pump, are shown in Figure S1 and discussed in the Supporting Information. The photon-drag effect already has been observed in metallic thin films due to an effective transfer of momentum from photons to electrons, thus creating a current along the direction of the propagation of light.[46,48] When the light is sent on the film with an angle of incidence different from 0°, the photon-drag current will travel parallel to the material surface and emits P-polarized THz light. A further bulk mechanism induced by a change in carrier direction caused by the Lorentz force[50] can be excluded. In fact, given the in-plane magnetic easy axis, the THz generation has been found to be independent from the crystal rotation. Finally, the THz polarization is almost independent by the pump linear polarization (see Figure S1), excluding a rectification process and thus a parity breaking due to strain in the thin-film geometry.

Pump polarization-dependent measurements are a useful probe to separately investigate the two generation mechanisms. Indeed, topological photocurrents are known to be sensitive to the circular polarization of light due to the circular photogalvanic effect (CPGE).[8,9] This dependence is explained in terms of an asymmetric depopulation of spin-polarized surface states by optical selection rules, generating a spin-polarized photocurrent.

Figure 2c shows the ratio $(E_{Cpol} - E_{Spol})/E_{Spol}$ for the three films, where E_{Cpol} and E_{Spol} are the THz (peak-to-peak) amplitude originating from the circularly and linearly (S-) polarized 800 nm pump, respectively. The ratio is negative for the 20 and 40 nm films, indicating a substantial contribution in the THz emission from the bulk states (as further discussed in the Supporting Information), and becomes positive in the 80 nm film, where topological surface states provide the major contribution, in agreement with previous results (see earlier). Figure 2d shows the ratio of the THz spectral amplitude generated by the 80 nm film between the circularly and linearly (S-pol) polarized pump signal. The bulk generation decreases slightly, while the sub-THz one emitted by the surface states improves, further supporting the picture of the two generation mechanisms. A possible contribution from the CPGE to the THz generation is also found in the 80 nm sample from the peak-to-peak values of the electric field, measured as a function of a quarter waveplate orientation α, converting the 800 nm pump from a linear to a circular polarization. Figure 2e shows how the THz generation follows a 2α behavior, as expected from a CPGE generation mechanism.[8,37,40]

Surface THz Emission. The polarization-dependent analysis shines a light on the bulk generation from the photon-drag effect. The photon-drag bulk generation mechanism highlights a major difference with respect to other topological semimetals (like TaAs) studied through THz emission spectroscopy.[37,38,40] There, the THz generation is dominated by the topological features of the bulk due to the breaking of parity symmetry. Instead, in Co_2MnGa, the

https://doi.org/10.1021/acsaelm.2c01376
ACS Appl. Electron. Mater. 2023, 5, 1437−1443

combination of surface plus bulk THz emission represents the major novelty, opening a route toward their application into tunable THz emitters.[40] However, the surface mechanisms giving rise to the sub-THz generation in the 80 nm sample are still not fully clear.

To improve the discussion on this topic, we performed THz emission measurements at normal incidence (where the photon-drag mechanism is ineffective), thus isolating the surface contribution from the bulk. We report the results in Figure 3 for the three films. The 20 and 40 nm films (red and

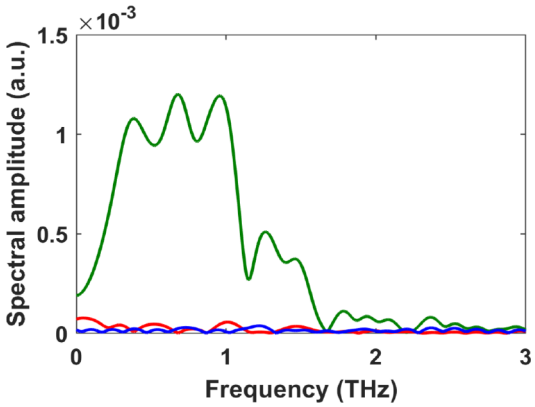

Figure 3. Normal incidence emission of CMG. Only the generation from the 80 nm sample can be resolved when the samples are pumped at normal incidence.

blue colored lines, respectively) have a negligible THz generation comparable to the background noise. The 80 nm film (green line) instead shows a huge emission below nearly 1 THz similar to that observed in Figure 2a. This result can be compared to the anomalous conductivity measurements performed on films of the same batch.[32] CMG films of thicknesses below 60 nm display a thickness-independent magnitude of the anomalous Hall conductivity (AHC).[32] For the 80 nm thick film instead, AHC increases ∼25% at 300 K due to an enhanced contribution from the topological surface states, as also supported by ab initio calculations.[32] Our results for the sub-THz generation show a behavior qualitatively similar to the AHC data as a function of thickness. The difference in the magnitude change between THz emission and AHC data can be addressed when considering that a simple relationship between the two quantities does not exist.[6] Indeed, AHC measurements sample the bulk topological properties of the films, while the THz emission includes contributions from the surface and bulk. On this line, ref 32 suggests that topological electronic states are fully formed, including Fermi arcs for the 80 nm thick film. Instead, for the 20 and 40 nm films having a lower AHC and a nearly zero sub-THz emission, the same paper suggests a deficiency in the topological surface states from which the photogalvanic current mainly takes place. These results and the THz polarization data reported earlier strongly suggest a topological origin of the sub-THz emission, as induced by photogalvanic effects from the surface states. Such a mechanism is predicted to take place as a consequence of interband transitions to the surface topological states.[51] However, theoretical and experimental results are scarce (due to the usual overwhelming bulk response), and only candidate materials like RhSi have been studied, predicting that Fermi arc photogalvanic currents can be perpendicular to the bulk injection currents regardless of the choice of materials surface.[52,53]

CONCLUSIONS

In this work we study the emission of THz radiation at room temperature from thin films of the cubic magnetic topological semimetal Co_2MnGa. The THz emission, at variance with others Weyl semimetals like TaAs where parity is not conserved, is generated by two microscopic mechanisms of different origin: a photon-drag mechanism of nontopological nature originating from the bulk of Co_2MnGa and providing a spectral range up to 3 THz, and a surface topological photogalvanic mechanism mainly responsible for the sub-THz emission. The photon-drag contribution that is present for a finite-incidence angle can be nearly canceled by working at normal incidence. The double emission mechanism has been further investigated by polarization-sensitive measurements. Indeed, by changing the pump polarization from linear to circular, we study the interplay between surface and bulk THz generation, supporting the topological nature of the surface THz emission. The overall THz signal generated by a 80 nm film has an efficiency per unit thickness hundreds of times higher than a conventional 500 μm thick ZnTe emitter.

The study of novel topological materials generating THz radiation is also important from a technological point of view. Recently there has been a shift in interest from semiconductors to semimetals for optical THz generation efficiency. While the latter can host well-known generation mechanisms like the photo−Dember[54] effect or optical rectification,[55] the mechanisms enabling THz generation in semimetals are still partially unknown. Indeed, over semiconductors, semimetals have the advantage of hosting topological quantum phases, allowing the production of tunable ultrafast photocurrents. In this framework, the investigation of the THz emission from Co_2MnGa adds an essential piece to the puzzle of THz technological cutting-edge research field.

ASSOCIATED CONTENT

Supporting Information

The Supporting Information is available free of charge at https://pubs.acs.org/doi/10.1021/acsaelm.2c01376.

Polarization properties of the emitted THz field and the surface vs bulk contribution (PDF)

AUTHOR INFORMATION

Corresponding Author

Stefano Lupi − *Department of Physics, Sapienza University, 00185 Rome, Italy; INFN − Laboratori Nazionali di Frascati, 00044 Frascati (Rome), Italy;* orcid.org/0000-0001-7002-337X; Email: stefano.lupi@roma1.infn.it

Authors

Luca Tomarchio − *Department of Physics, Sapienza University, 00185 Rome, Italy; INFN section of Rome, 00185 Rome, Italy;* orcid.org/0000-0003-0046-019X

Sen Mou − *INFN section of Rome, 00185 Rome, Italy;* orcid.org/0000-0002-6872-9389

Lorenzo Mosesso − *Department of Physics, Sapienza University, 00185 Rome, Italy;* orcid.org/0000-0002-5470-8659

https://doi.org/10.1021/acsaelm.2c01376
ACS Appl. Electron. Mater. 2023, 5, 1437−1443

Anastasios Markou − *Max Planck Institute for Chemical Physics of Solids, 01187 Dresden, Germany;* orcid.org/0000-0002-0812-6818

Edouard Lesne − *Max Planck Institute for Chemical Physics of Solids, 01187 Dresden, Germany*

Claudia Felser − *Max Planck Institute for Chemical Physics of Solids, 01187 Dresden, Germany*

Complete contact information is available at: https://pubs.acs.org/10.1021/acsaelm.2c01376

Author Contributions

The project has been conceptualized and supervised by S.L. and C.F. Samples have been synthesized and characterized by A.M. and E.L. THz emission measurements were carried out by L.T., S.M., and L.M. The data treatment was performed by L.T. All authors contributed to the writing of the paper.

Funding

The project has been funded through the PNRR MUR project PE0000023-NQSTI.

Notes

The authors declare no competing financial interest.

REFERENCES

(1) Mong, R. S. K.; Essin, A. M.; Moore, J. E. Antiferromagnetic topological insulators. *Phys. Rev. B* **2010**, *81*, 245209.

(2) Nagaosa, N.; Sinova, J.; Onoda, S.; MacDonald, A. H.; Ong, N. P. Anomalous Hall effect. *Rev. Mod. Phys.* **2010**, *82*, 1539.

(3) Chang, C.-Z.; Zhang, J.; Feng, X.; Shen, J.; Zhang, Z.; Guo, M.; Li, K.; Ou, Y.; Wei, P.; Wang, L.-L.; Ji, Z.-Q.; Feng, Y.; Ji, S.; Chen, X.; Jia, J.; Dai, X.; Fang, Z.; Zhang, S.-C.; He, K.; Wang, Y.; Lu, L.; Ma, X.-C.; Xue, Q.-K. Experimental Observation of the Quantum Anomalous Hall Effect in a Magnetic Topological Insulator. *Science* **2013**, *340* (6129), 167−170.

(4) Liu, E.; Sun, Y.; Kumar, N.; Muechler, L.; Sun, A.; Jiao, L.; Yang, S.-Y.; Liu, D.; Liang, A.; Xu, Q.; Kroder, J.; Süß, V.; Borrmann, H.; Shekhar, C.; Wang, Z.; Xi, C.; Wang, W.; Schnelle, W.; Wirth, S.; Chen, Y.; Goennenwein, S. T. B.; Felser, C. Giant anomalous Hall effect in a ferromagnetic kagome-lattice semimetal. *Nat. Phys.* **2018**, *14*, 1125−1131.

(5) Morimoto, T.; Zhong, S.; Orenstein, J.; Moore, J. E. Semiclassical theory of nonlinear magneto-optical responses with applications to topological Dirac/Weyl semimetals. *Phys. Rev. B* **2016**, *94*, 245121.

(6) Morimoto, T.; Nagaosa, N. Topological nature of nonlinear optical effects in solids. *Science Advances* **2016**, *2* (5), No. e1501524.

(7) Giorgianni, F.; Chiadroni, E.; Rovere, A.; Cestelli-Guidi, M.; Perucchi, A.; Bellaveglia, M.; Castellano, M.; Di Giovenale, D.; Di Pirro, G.; Ferrario, M.; Pompili, R.; Vaccarezza, C.; Villa, F.; Cianchi, A.; Mostacci, A.; Petrarca, M.; Brahlek, M.; Koirala, N.; Oh, S.; Lupi, S. Strong nonlinear terahertz response induced by Dirac surface states in Bi_2Se_3 topological insulator. *Nat. Commun.* **2016**, *7*, 11421.

(8) Chan, C.-K.; Lindner, N. H.; Refael, G.; Lee, P. A. Photocurrents in Weyl semimetals. *Phys. Rev. B* **2017**, *95*, No. 041104.

(9) de Juan, F.; Grushin, A. G.; Morimoto, T.; Moore, J. E. Quantized circular photogalvanic effect in Weyl semimetal. *Nat. Commun.* **2017**, *8*, 15995.

(10) Tokura, Y.; Yasuda, K.; Tsukazaki, A. Magnetic topological insulators. *Nature Reviews Physics* **2019**, *1*, 126−143.

(11) Hasan, M. Z.; Kane, C. L. Colloquium: Topological insulators. *Rev. Mod. Phys.* **2010**, *82*, 3045.

(12) Ortmann, F.; Roche, S.; Valenzuela, S. O. *Topological Insulators: Fundamentals and Perspectives*; Wiley-VCH Verlag GmbH & Co. KGaA: Weinheim, Germany, 2015; Vol. *12*, p 69469.

(13) Araki, Y. Magnetic Textures and Dynamics in Magnetic Weyl Semimetals. *Ann. Phys.* **2020**, *532* (2), 1900287.

(14) Destraz, D.; Das, L.; Tsirkin, S. S.; Xu, Y.; Neupert, T.; Chang, J.; Schilling, A.; Grushin, A. G.; Kohlbrecher, J.; Keller, L.; Puphal, P.; Pomjakushina, E.; White, J. S. Magnetism and anomalous transport in the Weyl semimetal PrAlGe: possible route to axial gauge fields. *npj Quantum Materials* **2020**, *5*, 5.

(15) Liu, D. F.; Liang, A. J.; Liu, E. K.; Xu, Q. N.; Li, Y. W.; Chen, C.; Pei, D.; Shi, W. J.; Mo, S. K.; Dudin, P.; Kim, T.; Cacho, C.; Li, G.; Sun, Y.; Yang, L. X.; Liu, Z. K.; Parkin, S. S. P.; Felser, C.; Chen, Y. L. Magnetic Weyl semimetal phase in a Kagome crystal. *Science* **2019**, *365*, 1282−1285.

(16) Finizio, S.; Kronenberg, A.; Vafaee, M.; Foerster, M.; Litzius, K.; de Lucia, A.; Menteş, T. O.; Aballe, L.; Krüger, B.; Jourdan, M.; Kläui, M. Magnetic configurations in nanostructured Co_2MnGa thin film elements. *New J. Phys.* **2015**, *17*, 083030.

(17) Zhu, Z.; Higo, T.; Nakatsuji, S.; Otani, Y. Magnetic and transport properties of amorphous, B2 and L21 Co: 2MnGa thin films. *AIP Advances* **2020**, *10*, 085020.

(18) Chang, G.; Xu, S.-Y.; Zhou, X.; Huang, S.-M.; Singh, B.; Wang, B.; Belopolski, I.; Yin, J.; Zhang, S.; Bansil, A.; Lin, H.; Hasan, M. Z. Topological Hopf and Chain Link Semimetal States and Their Application to Co_2MnGa. *Phys. Rev. Lett.* **2017**, *119*, 156401.

(19) Rhim, J.-W.; Kim, Y. B. Anisotropic density fluctuations, plasmons, and Friedel oscillations in nodal line semimetal. *New J. Phys.* **2016**, *18*, 043010.

(20) Belopolski, I.; Manna, K.; Sanchez, D. S.; Chang, G.; Ernst, B.; Yin, J.; Zhang, S. S.; Cochran, T.; Shumiya, N.; Zheng, H.; Singh, B.; Bian, G.; Multer, D.; Litskevich, M.; Zhou, X.; Huang, S.-M.; Wang, B.; Chang, T.-R.; Xu, S.-Y.; Bansil, A.; Felser, C.; Lin, H.; Hasan, M. Z. Discovery of topological Weyl fermion lines and drumhead surface states in a room temperature magnet. *Science* **2019**, *365* (6459), 1278−1281.

(21) Burkov, A. A.; Hook, M. D.; Balents, L. Topological nodal semimetals. *Phys. Rev. B* **2011**, *84*, 235126.

(22) Fang, C.; Weng, H.; Dai, X.; Fang, Z. Topological nodal line semimetals. *Chinese Phys. B* **2016**, *25*, 117106.

(23) Tai, T.; Lee, C. H. Anisotropic nonlinear optical response of nodal-loop materials. *Phys. Rev. B* **2021**, *103*, 195125.

(24) Ahn, S.; Mele, E. J.; Min, H. Electrodynamics on Fermi Cyclides in Nodal Line Semimetals. *Phys. Rev. Lett.* **2017**, *119*, 147402.

(25) Carbotte, J. P. Optical response of a line node semimetal. *J. Phys.: Condens. Matter* **2017**, *29*, 045301.

(26) Kurtulus, Y.; Dronskowski, R.; Samolyuk, G. D.; Antropov, V. P. Electronic structure and magnetic exchange coupling in ferromagnetic full Heusler alloys. *Phys. Rev. B* **2005**, *71*, 014425.

(27) Manna, K.; Muechler, L.; Kao, T.-H.; Stinshoff, R.; Zhang, Y.; Gooth, J.; Kumar, N.; Kreiner, G.; Koepernik, K.; Car, R.; Kübler, J.; Fecher, G. H.; Shekhar, C.; Sun, Y.; Felser, C. From Colossal to Zero: Controlling the Anomalous Hall Effect in Magnetic Heusler Compounds via Berry Curvature Design. *Phys. Rev. X* **2018**, *8*, 041045.

(28) Faregh, R. A.; Boochani, A.; Masharian, S. R.; Jafarpour, F. H. The surface effect on the thermodynamic stability, half-metallic and optical properties of $Co_2MnGa(001)$ films: a DFT study. *International Nano Letters* **2019**, *9*, 339−348.

(29) Rhee, J. Y.; Kudryavtsev, Y. V.; Kim, K. W.; Lee, Y. P. Peculiar Optical Properties of Co_2MnGa Alloys. *ASEAN Journal on Science & Technology for Development* **2007**, *24*, 1−2.

(30) Swekis, P.; Sukhanov, A. S.; Chen, Y.-C.; Gloskovskii, A.; Fecher, G. H.; Panagiotopoulos, I.; Sichelschmidt, J.; Ukleev, V.; Devishvili, A.; Vorobiev, A.; Inosov, D. S.; Goennenwein, S. T. B.; Felser, C.; Markou, A. Magnetic and Electronic Properties of Weyl Semimetal Co_2MnGa Thin Films. *Nanomaterials* **2021**, *11* (1), 251.

(31) Lee, C. H.; Yap, H. H.; Tai, T.; Xu, G.; Zhang, X.; Gong, J. Enhanced higher harmonic generation from nodal topology. *Phys. Rev. B* **2020**, *102*, 035138.

(32) Markou, A.; Kriegner, D.; Gayles, J.; Zhang, L.; Chen, Y.-C.; Ernst, B.; Lai, Y.-H.; Schnelle, W.; Chu, Y.-H.; Sun, Y.; Felser, C.

Thickness dependence of the anomalous Hall effect in thin films of the topological semimetal Co_2MnGa. *Phys. Rev. B* **2019**, *100*, 054422.
(33) Reichlova, H.; Schlitz, R.; Beckert, S.; Swekis, P.; Markou, A.; Chen, Y.-C.; Kriegner, D.; Fabretti, S.; Hyeon Park, G.; Niemann, A.; Sudheendra, S.; Thomas, A.; Nielsch, K.; Felser, C.; Goennenwein, S. T. B. Large anomalous Nernst effect in thin films of the Weyl semimetal Co_2MnGa. *Appl. Phys. Lett.* **2018**, *113*, 212405.
(34) Sakai, A.; Mizuta, Y. P.; Nugroho, A. A.; Sihombing, R.; Koretsune, T.; Suzuki, M.-T.; Takemori, N.; Ishii, R.; Nishio-Hamane, D.; Arita, R.; Goswami, P.; Nakatsuji, S. Giant anomalous Nernst effect and quantum-critical scaling in a ferromagnetic semimetal. *Nat. Phys.* **2018**, *14*, 1119−1124.
(35) Han, X.; Markou, A.; Stensberg, J.; Sun, Y.; Felser, C.; Wu, L. Giant intrinsic anomalous terahertz Faraday rotation in the magnetic Weyl semimetal Co_2MnGa at room temperature. *Phys. Rev. B* **2022**, *105*, 174406.
(36) Bierhance, G.; Markou, A.; Gueckstock, O.; Rouzegar, R.; Behovits, Y.; Chekhov, A. L.; Wolf, M.; Seifert, T. S.; Felser, C.; Kampfrath, T. Spin-voltage-driven efficient terahertz spin currents from the magnetic Weyl semimetals Co_2MnGa and Co_2MnAl. *Appl. Phys. Lett.* **2022**, *120*, 082401.
(37) Sun, K.; Sun, S.-S.; Wei, L.-L.; Guo, C.; Tian, H.-F.; Chen, G.-F.; Yang, H.-X.; Li, J.-Q. Circular Photogalvanic Effect in the Weyl Semimetal TaAs. *CHIN. PHYS. LETT.* **2017**, *34* (11), 117203.
(38) Sirica, N.; Tobey, R. I.; Zhao, L. X.; Chen, G. F.; Xu, B.; Yang, R.; Shen, B.; Yarotski, D. A.; Bowlan, P.; Trugman, S. A.; Zhu, J.-X.; Dai, Y. M.; Azad, A. K.; Ni, N.; Qiu, X. G.; Taylor, A. J.; Prasankumar, R. P. Tracking Ultrafast Photocurrents in the Weyl Semimetal TaAs Using THz Emission Spectroscopy. *Phys. Rev. Lett.* **2019**, *122*, 197401.
(39) Tong, M.; Hu, Y.; Xie, X.; Zhu, X.; Wang, Z.; Cheng, X.; Jiang, T. Helicity-dependent THz emission induced by ultrafast spin photocurrent in nodal-line semimetal candidate Mn_3Bi_2. *Opto-Electron. Adv.* **2020**, *3*, 200023.
(40) Gao, Y.; Kaushik, S.; Philip, E. J.; Li, Z.; Qin, Y.; Liu, Y. P.; Zhang, W. L.; Su, Y. L.; Chen, X.; Weng, H.; Kharzeev, D. E.; Liu, M. K.; Qi, J. Chiral terahertz wave emission from the Weyl semimetal TaAs. *Nat. Commun.* **2020**, *11*, 720.
(41) Hamh, S. Y.; Park, S.-H.; Han, J.; Jeon, J. H.; Kahng, S.-J.; Kim, S.; Choi, S.-H.; Bansal, N.; Oh, S.; Park, J.; Kim, J. S.; Kim, J. M.; Noh, D. Y.; Lee, J. S. Anisotropic Terahertz Emission from Bi_2Se_3 Thin Films with Inclined Crystal Planes. *Nanoscale Res. Lett.* **2015**, *10*, 489.
(42) Zhu, L.-G.; Kubera, B.; Fai Mak, K.; Shan, J. Effect of Surface States on Terahertz Emission from the Bi_2Se_3 Surface. *Sci. Rep.* **2015**, *5*, 10308.
(43) Strait, J. H.; Holland, G.; Zhu, W.; Zhang, C.; Ilic, B. R.; Agrawal, A.; Pacifici, D.; Lezec, H. J. Revisiting the Photon-Drag Effect in Metal Films. *Phys. Rev. Lett.* **2019**, *123*, 053903.
(44) Obraztsov, P. A.; Kanda, N.; Konishi, K.; Kuwata-Gonokami, M.; Garnov, S. V.; Obraztsov, A. N.; Svirko, Y. P. Photon-drag-induced terahertz emission from graphene. *Phys. Rev. B* **2014**, *90*, No. 241416.
(45) Zhukova, M.; Makarov, E.; Putilin, S.; Tsypkin, A.; Chegnov, V.; Chegnova, O.; Bespalov, V. Experimental study of THz electro-optical sampling crystals ZnSe, ZnTe and GaP. *Journal of Physics: Conference Series* **2017**, *917*, 062021.
(46) Goff, J. E.; Schaich, W. L. Theory of the photon-drag effect in simple metals. *Phys. Rev. B* **2000**, *61*, 10471.
(47) Shalygin, V. A.; Moldavskaya, M. D.; Danilov, S. N.; Farbshtein, I. I.; Golub, L. E. Circular photon drag effect in bulk semiconductors. *J. Phys.: Conf. Ser.* **2017**, *864*, 012072.
(48) Mikheev, G. M.; Saushin, A. S.; Styapshin, V. M.; Svirko, Y. P. Interplay of the photon drag and the surface photogalvanic effects in the metal-semiconductor nanocomposite. *Sci. Rep.* **2018**, *8*, 8644.
(49) Maysonnave, J.; Huppert, S.; Wang, F.; Maero, S.; Berger, C.; de Heer, W.; Norris, T. B.; De Vaulchier, L. A.; Dhillon, S.; Tignon, J.; Ferreira, R.; Mangeney, J. Terahertz generation by dynamical photon drag effect in graphene. *Nano Lett.* **2014**, *14* (10), 5797−5802.
(50) Héroux, J. B.; Ino, Y.; Kuwata-Gonokami, M.; Hashimoto, Y.; Katsumoto, S. Terahertz radiation emission from GaMnAs. *Appl. Phys. Lett.* **2006**, *88*, 221110.
(51) Cao, J.; Wang, M.; Yu, Z.-M.; Yao, Y. Bulk Fermi arc transition induced large photogalvanic effect in Weyl semimetals. *Phys. Rev. B* **2022**, *106*, 125416.
(52) Chang, G.; Yin, J.-X.; Neupert, T.; Sanchez, D. S.; Belopolski, I.; Zhang, S. S.; Cochran, T. A.; Chéng, Z.; Hsu, M.-C.; Huang, S.-M.; Lian, B.; Xu, S.-Y.; Lin, H.; Hasan, M. Z. Unconventional Photocurrents from Surface Fermi Arcs in Topological Chiral Semimetals. *Phys. Rev. Lett.* **2020**, *124*, 166404.
(53) Rees, D.; Lu, B.; Sun, Y.; Manna, K.; Özgür, R.; Subedi, S.; Borrmann, H.; Felser, C.; Orenstein, J.; Torchinsky, D. H. Direct Measurement of Helicoid Surface States in RhSi Using Nonlinear Optics. *Phys. Rev. Lett.* **2021**, *127*, 157405.
(54) Apostolopoulos, V.; Barnes, M. E. THz emitters based on the photo-Dember effect. *J. Phys. D: Appl. Phys.* **2014**, *47*, 374002.
(55) Khurgin, J. B. Optical rectification and terahertz emission in semiconductors excited above the band gap. *Journal of the Optical Society of America B* **1994**, *11* (12), 2492−2501.

https://doi.org/10.1021/acsaelm.2c01376
ACS Appl. Electron. Mater. 2023, 5, 1437−1443